

Isovector splitting of nucleon effective masses, ab-initio benchmarks and extended stability criteria for Skyrme energy functionals

T. Lesinski,^{1,*} K. Bennaceur,^{1,2} T. Duguet,³ and J. Meyer¹

¹ Institut de Physique Nucléaire de Lyon, CNRS-IN2P3/Université Claude Bernard Lyon 1, 43, bd. du 11 novembre 1918, F-69622 Villeurbanne Cedex, France

² CEA-Saclay DSM/DAPNIA/SPhN, F-91191 Gif-sur-Yvette, France

³ National Superconducting Cyclotron Laboratory and Department of Physics and Astronomy, Michigan State University, East Lansing, MI 48824, USA

(Dated: 1st September 2018)

We study the effect of the splitting of neutron and proton effective masses with isospin asymmetry on the properties of the Skyrme energy density functional. We discuss the ability of the latter to predict observable of infinite matter and finite nuclei, paying particular attention to controlling the agreement with ab-initio predictions of the spin-isospin content of the nuclear equation of state, as well as diagnosing the onset of finite size instabilities, which we find to be of critical importance. We show that these various constraints cannot be simultaneously fulfilled by the standard Skyrme force, calling at least for an extension of its P-wave part.

PACS numbers: 21.30.Fe, 21.60.Jz

I. INTRODUCTION

In the study of medium to heavy mass nuclei, nuclear Energy Density Functional (EDF) approaches, based on self-consistent Hartree-Fock (HF) methods and their extensions, constitute the theoretical tool of choice [1]. Thanks to the development of better energy functionals and to the increase of computer resources, nuclear EDF is on the edge of becoming a predictive theory for all nuclei but the lightest. This is not only true for ground state properties, such as binding energies, radii or multipoles of the density, but also for low-energy spectroscopy and decay probabilities [1].

However, the accuracy and predictive power needed for unknown regions of the nuclear chart still leave a lot of room for improvement. The phenomenological nature of Skyrme functionals makes their ability to faithfully predict observable or phenomena not linked with those used for their construction quite weak. Indeed, the limited number of adjustable parameters (compared to the wealth of nuclear observable to be matched) turns fitting a Skyrme functional into an overconstrained problem (which, of course, does not prevent some parts of it from being underconstrained).

As a direct consequence, many properties of existing parameterizations are biased to the fitting procedure and the limited analytical form of the Skyrme force, rather than to physical reasoning. A well-known example is the equation of state (EOS) of Pure Neutron Matter (PNM), which is sometimes subject to a pathological collapse at high density when not explicitly constrained. This is problematic insofar as one of the major challenges of contemporary nuclear theory is to predict properties of very isospin asymmetric nuclear systems, *i.e.* neutron rich nu-

clei and matter in neutron stars. Experimental data being unavailable in this domain of isospin, one has started relying on ab-initio theoretical results to constrain isovector properties of the functional. It has led to the construction of the “Saclay-Lyon” SLy series of parameterizations [2, 3, 4] by fitting (among other quantities) a theoretical equation of state of neutron matter.

Isovector features of the nuclear EOS are crucial for a good understanding of neutron stars, exotic nuclear collisions produced at radioactive beam facilities and to describe the structure of exotic nuclei. For instance, the density dependence of the volume symmetry energy determines the proton fraction in β equilibrium in neutron stars, which ultimately drives the cooling rate and neutrino emission [5]. The high-density part of the symmetry energy, which happens to be strongly model dependent, also influences significantly the isospin diffusion in heavy-ion collisions [6]. Finally, the low-density part of the symmetry energy is correlated with the size of neutron skins in finite nuclei [7].

Beyond global isospin-dependent properties of the EOS, the isovector part of nucleon-dependent quantities may influence the behavior of the above mentioned systems. Thus, collision observable depend on the momentum dependence of the mean-field, in particular on its isovector component [8, 9]. Also, some properties of neutron stars require a precise knowledge of isoscalar and isovector nucleon effective masses [10, 11]. The latter, which drives the *splitting of neutron and proton effective masses* with neutron/proton asymmetry, will serve as a starting point for our study. Indeed, a lot of efforts has recently been devoted to the microscopic characterization of neutron and proton effective masses in infinite Asymmetric Nuclear Matter (ANM) [12, 13, 14, 15, 16, 17, 18, 19, 20, 21]. Either in ANM or in nuclei, the two species acquire different effective masses. This property is quantified by the difference $\Delta m^*(I) = m_n^*(I) - m_p^*(I)$, where $I = (\rho_n - \rho_p)/(\rho_n + \rho_p)$

*Electronic address: lesinski@ipnl.in2p3.fr

is the isospin asymmetry while ρ_n and ρ_p denote neutron and proton densities, respectively. Note that the different effective masses m^* discussed in the text always refer in fact to the ratio m^*/m , where m is the bare nucleon mass. The latter is taken to be the same for neutrons and protons.

This effective-mass splitting, though, is only one of a wealth of observable which can be subject to comparison between ab-initio predictions and EDF models. In this work we present results of a classical yet long unused test: the separation of infinite Symmetric Nuclear Matter (SNM) potential energy per particle into spin-isospin channels.

We shall also pay particular attention to controlling instabilities (*i.e.* non-physical spontaneous breaking of spin, isospin and/or spatial symmetries), and correlate $\Delta m^*(I)$ with *vector* properties of the functional. We thus investigate the behavior of the latter with respect to the breaking of time-reversal invariance and the onset of spin polarization, looking for an overall consistency check of its spin-isospin content. Indeed, such properties will become more and more important as one attempts to use full-fledged Skyrme functionals to study odd-mass nuclei, calculate rotational properties through self-consistent cranking calculations, or use more general dynamical methods [22].

This paper is organized as follows: in section II we present the set of Skyrme parameterizations used in this study and examine basic properties of nuclear matter and finite nuclei. From then, in section III we perform a more detailed study of the spin-isospin content of the functionals and of their stability against finite-size spin and isospin perturbations using response functions in the Random Phase Approximation (RPA).

II. CONSTRAINING THE ISOVECTOR EFFECTIVE MASS

The nucleon effective mass m^* is a key property characterizing the propagation of (quasi)nucleons through the nuclear medium [23]. It is a reminder of the non-locality and energy dependence of the nucleon self-energy $\Sigma(k, \epsilon)$, themselves originating from the finite range and non-locality in time and space of the nucleon-nucleon interaction. Mean-field-like theories of finite nuclei or infinite matter assume an on-shell propagation of the nucleons. The effective mass associated with such an on-shell propagation does not take into account the fragmentation of the single-particle strength and thus, a limited part of the effects associated with the energy dependence of $\Sigma(k, \epsilon)$. Finally, the total energy is calculated by considering the quasi-holes (particles) to have spectroscopic factors of 1. In this context, either microscopic [24] or making use of phenomenological interactions or functionals [1], mean-field methods do not correspond to a naive Hartree-Fock theory and always amount to renormalizing a certain class of correlations into the effective vertex. However,

the energy dependence of the self-energy arising from the correlations only influences the position of the quasi-particle peak energy. The standard nuclear EDF methods differ in several respects from Kohn-Sham Density Functional Theory [25]. In particular, the strategy usually followed in the former is to leave room for improvement through further inclusions of correlations. This can be done by performing (Quasiparticle)-Random-Phase-Approximation (QRPA) calculations [26, 27] or by employing the Generator Coordinate Method (GCM) on top of symmetry-restored mean-field states [28].

Thus, the effective mass adjusted at the pure mean-field level is not expected to generate single-particle spectra matching exactly experimental data extracted from neighboring odd-mass nuclei. In particular, the coupling of single-particle motions to surface vibrations in closed-shell nuclei is known to increase the density of states at the Fermi surface and thus the effective mass [29, 30]. A mean-field isoscalar effective mass m_s^* lying in the interval 0.7/0.8 in SNM, is able to account for a good reproduction of both isoscalar quadrupole giant resonances data in doubly closed-shell nuclei [31] and of single-particle spectra in neighboring ones provided particle-vibration coupling has been properly included. When the latter coupling is taken into account, the effective mass becomes greater than one for states near the Fermi surface. Certainly, a lot remains to be done to understand these features microscopically in more involved cases [32]. This is not only true for mid-shell nuclei where the coupling to both rotational and vibrational states can be important, but also for exotic nuclei where the coupling to the continuum becomes crucial and where shape coexistence and/or large amplitude motion appear more systematically.

In very exotic systems, the isovector behavior of m_p^* and m_n^* should play an important role. However, so far, no experimental data from finite nuclei has allowed a determination of the effective mass splitting as a function of neutron richness. In this context, ab-initio calculations of ANM are of great help. Non-relativistic Brueckner-Hartree-Fock (BHF) calculations, with or without three-body force, and, with or without rearrangement terms in the self-energy, predicted $\Delta m^*(I)$ to be such that $m_n^* \geq m_p^*$ in neutron-rich matter, that is, for $I \geq 0$. Such a conclusion was also reached by calculating the energy dependence of the symmetry potential (the Lane potential [33]) within a phenomenological formalism [8]. The latter result was confirmed by microscopic Dirac-Brueckner-Hartree-Fock (DBHF) calculations [34]. The situation regarding the prediction of the effective mass splitting was complexified due to an apparent contradiction between results obtained from BHF [12, 14] and DBHF calculations [16]. However, the situation was finally clarified in Ref. [19, 20] where the importance of the energy dependence of the self-energy and the need to compare the non-relativistic effective mass with the vector effective mass in the relativistic framework [35] were pointed out.

Thus, the sign of the splitting is rather solidly predicted. However, its amplitude is subject to a much greater uncertainty. Starting from that observation, the goal of the present section is to study the impact of the effective-mass splitting on properties of exotic nuclei predicted by Skyrme-Hartree-Fock calculations. As far as the effective-mass splitting is concerned, one expects consequences onto structure properties of neutron-rich nuclei. As a relatively large asymmetry may be necessary to reveal the influence of the splitting, data from nuclei not yet studied experimentally should provide crucial information in that respect. As the effective mass governs the density of states at the Fermi surface (together with the spin-orbit and the tensor forces), the amplitude of the splitting may influence properties such as masses and single particle properties of exotic nuclei, the evolution of isotopic shifts across neutron rich closed-shell nuclei or shell corrections in superheavy nuclei around the ($N = 184, Z = 120$) island of stability [36, 37, 38, 39]. Also, neutron and proton correlations beyond the mean-field should develop rather differently depending on the direction and amplitude of the effective-mass splitting. This could be true for static and dynamical pairing correlations as well as for the coupling to vibrational and rotational states. Finally, the effective mass splitting should leave its fingerprint onto the characteristics of isovector vibrational states of different sorts in neutron rich nuclei [40].

A. Fitting protocol

Trying to keep a coherence in the way we construct Skyrme functionals, we take the fitting protocol used to define the SLy forces [2, 3, 4] as a basis for the present work. Also, we pay attention to the fact that any improved or complexified functional includes all features validated by the SLy ones.

The SLy functionals were derived from an effective interaction, that is, time-odd components of the functional are eventually linked to time-even ones. However, some terms in the functional given by Eqs. A6a-A6d were dropped for some of the parameterizations. For instance, time-odd terms of the form $\mathbf{s}_q \cdot \Delta\mathbf{s}_{q'}$ have not been considered when calculating odd nuclei [41] or rotational states [42]. Also, \mathbb{J}^2 contributions to the energy functional associated with momentum-dependent terms in the central Skyrme force have been omitted for some of the SLy parameterizations, as it has been the case for most of the Skyrme functionals so far [1]. Rigorously, omitting terms is inconsistent with the idea of deriving a functional from an interaction. In any case, the latter approach is only used for simplicity until proper adjustment or derivation of time-odd terms is feasible. We refer the reader to Refs. [1, 2, 3, 4] for a more extensive discussion on the subject. We presently take the SLy5 parameterization as a starting point. Thus, the two-body part of the center of mass correction is omitted whereas the \mathbb{J}^2

terms are fully kept. The spin-orbit term is the standard one, with a single parameter adjusted on the splitting of the $3p$ neutron level in ^{208}Pb .

Within this general scheme, we have built a series of three new Skyrme forces, denoted hereafter f_- , f_0 and f_+ . The departures from the SLy protocol considered presently are (i) a better control of spin-isospin instabilities via Landau parameters (ii) the use of two density-dependent zero-range terms [43] (iii) a constraint on the isovector effective mass, such that, in neutron-rich systems, $m_n^* < m_p^*$ for f_- , $m_n^* = m_p^*$ for f_0 and $m_n^* > m_p^*$ for f_+ .

With two density dependent terms, the compressibility and the isoscalar effective mass are no longer bound together and can be chosen independently. However, this is not directly used here and an isoscalar effective mass of $m_s^* = 0.7$, close to the SLy5 value, is chosen for the three parameterizations f_-, f_0, f_+ . The additional freedom brought about by the second density-dependent term is only used to adjust more easily the high-density part of the PNM EOS (see below). In the end, the only parameter subject to variation between f_- , f_0 and f_+ is the isovector effective mass m_v^* which, m_s^* being constant, drives the splitting $\Delta m^*(I)$.

In the present work, we use the SLy5 force as a reference, and include a comparison with the recently proposed LNS parameterization [44] which was also built to match the splitting of effective masses and the neutron matter EOS predicted by BHF calculations. The SkP force [45], initially built for the study of pairing effects, will be used for a special purpose in the discussion about instabilities.

B. Elementary properties of studied forces

As we focus on the behavior of effective masses m_q^* with isospin asymmetry, we recall that these quantities are related to the dependence of the energy density functional, Eqs. A6a–A6d, on kinetic densities τ_q , as

$$\frac{\hbar^2}{2m_q^*(I)} = \frac{\partial \mathcal{H}}{\partial \tau_q} = \frac{\hbar^2}{2m} + C_0^\tau \rho_0 + qI C_1^\tau \rho_0 \quad (1a)$$

$$\frac{m}{m_q^*(I)} \equiv \frac{m}{m_s^*} + qI \left(\frac{m}{m_s^*} - \frac{m}{m_v^*} \right) \quad (1b)$$

where ρ_0 is the scalar-isoscalar density and $q = +1, -1$ respectively for neutrons and protons (for the definition of C_t^τ coefficients, see appendix A). The splitting of effective masses, quantified by

$$\frac{\Delta m^*(I)}{m} = \frac{m_n^*(I)}{m} - \frac{m_p^*(I)}{m}, \quad (2)$$

is governed by the isoscalar and isovector effective masses

$$\frac{m}{m_s^*} = 1 + \frac{2m}{\hbar^2} C_0^\tau \rho_0 \equiv 1 + \kappa_s, \quad (3a)$$

$$\frac{m}{m_v^*} = 1 + \frac{2m}{\hbar^2} (C_0^\tau - C_1^\tau) \rho_0 \equiv 1 + \kappa_v. \quad (3b)$$

We use the usual convention for the isovector effective mass, which stems from its definition through the enhancement factor κ_v of the Thomas-Reiche-Kuhn sum rule [46]. However, m_v^* and κ_v are *not* isovector quantities in the sense of isovector couplings of the functional.

In the following, we shall discuss the value of $\Delta m^*(I)$ at $I = 1$, which we note Δm^* in the following, for the sake of brevity. We have

$$\frac{\Delta m^*}{m} = \frac{2(\kappa_v - \kappa_s)}{(1 + \kappa_s)^2 - (\kappa_v - \kappa_s)^2}, \quad (4)$$

such that $\Delta m^* > 0$ for $\kappa_v > \kappa_s$, or equivalently $m_v^* < m_s^*$, or $C_1^\tau < 0$.

Table I: Infinite nuclear matter properties of the Skyrme forces quoted in the text. The quantities ρ_{sat} and E/A denote the density and energy per particle at saturation in SNM. The symmetry energy and the compressibility (for symmetric matter) are respectively 32 MeV and 230 MeV for SLy5 and all f_x forces. In the case where $m_s^* \sim 0.7$, $\kappa_s \sim 0.43$, so we have $\Delta m^* > 0$ if $\kappa_v \gtrsim 0.43$.

Force	ρ_{sat}	E/A	m_s^*	κ_v	m_v^*	Δm^*
SLy5	0.161	-15.987	0.697	0.25	0.800	-0.182
f_-	0.162	-16.029	0.700	0.15	0.870	-0.284
f_0	0.162	-16.035	0.700	0.43	0.700	0.001
f_+	0.162	-16.036	0.700	0.60	0.625	0.170
LNS	0.175	-15.320	0.825	0.38	0.727	0.227
SkP	0.170	-16.590	1.030	0.32	0.760	0.418

Bulk properties of f_x parameterizations are displayed in Table I. We note that, while the position of the saturation point varies little between our forces (SLy5 and f_x), this consistency is lost in the case of LNS and SkP. These properties depend on the observable used in the fitting procedure. In the case of LNS, the saturation point relates to an Extended Brueckner-Hartree-Fock (EBHF) calculation [14], predicting values of $(E/A)_{\text{sat}}$ and ρ_{sat} which are larger than empirical ones. A similar but lesser trend is observed for SkP. In this case it seems to be correlated with the choice of effective masses and their interplay with other parameters of the force. Indeed, binding energies computed with SkP compare satisfactorily with experimental ones, while LNS suffers in this respect from the lack of readjustment of the saturation point on nuclear data. As it has been shown in Ref. [47], nuclear binding energies are highly sensitive to the choice of the energy at saturation, which is therefore constrained to a very tight interval if one wants to reproduce such quantities. This constraint is especially tight compared to the uncertainty of ab-initio predictions. Despite the fit of surface properties ($C_0^{\Delta\rho}$ parameter) on a set of nuclear data, the accuracy of binding energies predicted by LNS is of the order of 5%, to be compared with less than 1% for SLy5.

C. Properties of the nuclear matter EOS

It is interesting to note that SLy parameterizations were fitted to PNM EOS with the idea of improving isospin properties of the functionals. One consequence was to generate functionals with $\Delta m^* < 0$, in opposition to ab-initio predictions. On the other hand, older functionals such as SIII [48] and SkM* [49], which were not fitted to PNM, had $\Delta m^* > 0$. The same exact situation happens for the Gogny force [50]. Thus, improving global isovector properties (EOS) seems to deteriorate those related to single-particle states (m_v^*) with currently used functionals. This can be better understood by examining the expressions for SNM and PNM EOS:

$$\begin{aligned} \frac{E}{A}(\rho_0, I = 0) &= \frac{3}{5} \frac{\hbar^2}{2m} \left(\frac{3\pi^2}{2} \right)^{2/3} \rho_0^{2/3} + C_0^\rho(\rho_0) \rho_0 \\ &+ C_0^\tau \frac{3}{5} \left(\frac{3\pi^2}{2} \right)^{2/3} \rho_0^{5/3}, \end{aligned} \quad (5a)$$

$$\begin{aligned} \frac{E}{A}(\rho_0, I = 1) &= \frac{3}{5} \frac{\hbar^2}{2m} (3\pi^2)^{2/3} \rho_0^{2/3} \\ &+ [C_0^\rho(\rho_0) + C_1^\rho(\rho_0)] \rho_0 \\ &+ [C_0^\tau + C_1^\tau] \frac{3}{5} (3\pi^2)^{2/3} \rho_0^{5/3}. \end{aligned} \quad (5b)$$

If $C_t^\rho(\rho_0)$ coefficients only contain one low power of the density ($\propto \rho_0^{1/6}$), the latter influences low-density parts of the EOS more than high-density ones. The effective mass term then determines the high-density part of the EOS. In SNM, this translates into the well-known relation between m_s^* and the incompressibility K_∞ [2, 3, 4]. In the case of PNM, the EOS above ρ_{sat} is then mostly fixed by the term proportional to $C_0^\tau + C_1^\tau$ in Eq. (5b), and any attempt to use the density dependence to counteract its effects, results in a very strong constraint on the latter. This in turn degrades the behavior of the functional at and below saturation density and the fit to properties of finite nuclei. We recall at this point that the condition $\Delta m^* > 0$ corresponds to $C_1^\tau < 0$, which drives the high-density PNM EOS down and explains why usual Skyrme functionals predict either a collapse of the PNM EOS if $\Delta m^* > 0$, or, like the SLy functionals fitted to PNM EOS, the wrong sign of the effective mass splitting in neutron rich matter.

If $C_t^\rho(\rho_0)$ coefficients contain an additional density dependence with a higher power, the previous discussion does not apply: using two density-dependent terms in the functional ($\propto \rho_0^{1/3}; \rho_0^{2/3}$) [43] allowed us to construct (f_- , f_0 , f_+) with a good fit to PNM EOS, a free choice of effective masses and satisfactory nuclear properties.

The previous discussion already shows the type of problems and information arising from our attempt to improve on the fitting protocol of SLy functionals by using more inputs from ab-initio calculations. Now, Fig. 1 shows SNM and PNM EOS as obtained from (f_- , f_0 , f_+ , SLy5) and as predicted by Variational Chain Sum-

mation (VCS) methods [51]. At this point, one can see that the four forces (f_- , f_0 , f_+ , SLy5) reproduce both microscopic EOS with the same accuracy. However, it remains to be seen whether or not this translates into identical global spin-isospin properties and into similar nuclear structure properties.

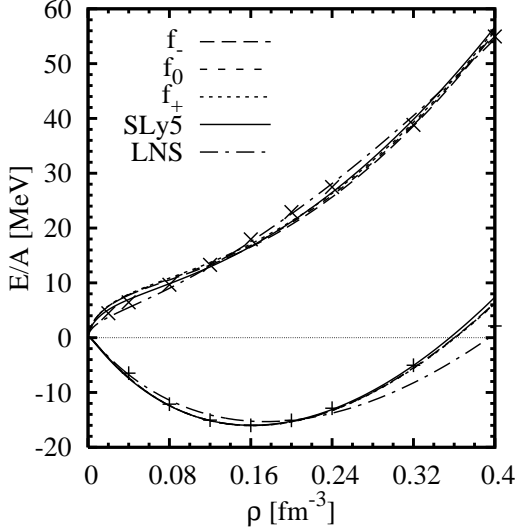


Figure 1: SNM and PNM EOS as given by Skyrme functionals presently discussed (see text), compared with VCS results by Akmal *et al.* [51] (crosses: PNM, plusses: SNM).

D. Effects on properties of nuclei

We now study the effects of the variation of the isovector effective mass on selected properties of spherical nuclei. We start with HF single-particle energies, then binding energies, ending with a short sum-rule based analysis of isovector giant resonances.

For computations of open-shell nuclei, we use, in the particle-particle channel, a zero-range interaction with a density dependent (mixed surface and volume) form factor defined as:

$$V_{\text{pair}}(\mathbf{R}, \mathbf{r}) = V_0 \delta(\mathbf{r}) \left[1 - \frac{\rho_0(\mathbf{R})}{2\rho_{\text{sat}}} \right], \quad (6)$$

where $\mathbf{R} = (\mathbf{r}_1 + \mathbf{r}_2)/2$ and $\mathbf{r} = \mathbf{r}_1 - \mathbf{r}_2$. The local HFB equations are renormalized following the procedure developed in Ref. [52].

The strength V_0 is adjusted to the mean pairing gaps of six semi-magic nuclei (neutron gaps in ^{120}Sn , ^{198}Pb , ^{212}Pb and proton gaps in ^{92}Mo , ^{144}Sm and ^{212}Rn). In this procedure we compute theoretical spectral gaps defined as $\Delta_{th} = \text{Tr}(\tilde{h}\tilde{\rho})/\text{Tr}(\tilde{\rho})$, where \tilde{h} is the pairing field and $\tilde{\rho}$ the pairing density [45], and adjust each of them upon an experimental gap extracted through a five point difference formula from masses of neighboring nuclei, as suggested in Ref. [53].

1. Single-particle energies

Effective masses are known to control the average density of single-particle states. It is thus interesting to check to what extent such statement applies to neutron-rich nuclei when varying m_v^* . In this part of the study, we are mainly interested in evaluating the change in the single-particle energies generated by the functional for different splittings and not directly by a comparison with experimental results.

Single-particle energies in ^{132}Sn and ^{208}Pb are plotted on Fig. 2. The general trend followed by neutron states with increasing Δm^* (from force f_- to f_+) corresponds to an increase of the density of neutron states: they tend to come closer to the Fermi energy ε_F ; notable exceptions being both neutron $1i$ levels in ^{208}Pb . The opposite behavior is observed in proton levels, which spread away from ε_F with increasing Δm^* (except for the proton $1h_{11/2}$ level). However, these trends are rather marginal, which can be linked with the moderate bulk asymmetry of these nuclei ($I = (N - Z)/A = 0.24$ for ^{132}Sn and 0.21 for ^{208}Pb). This moderate asymmetry means that the isovector term in the definition of the effective mass (Eq. (1b)) is weakly probed.

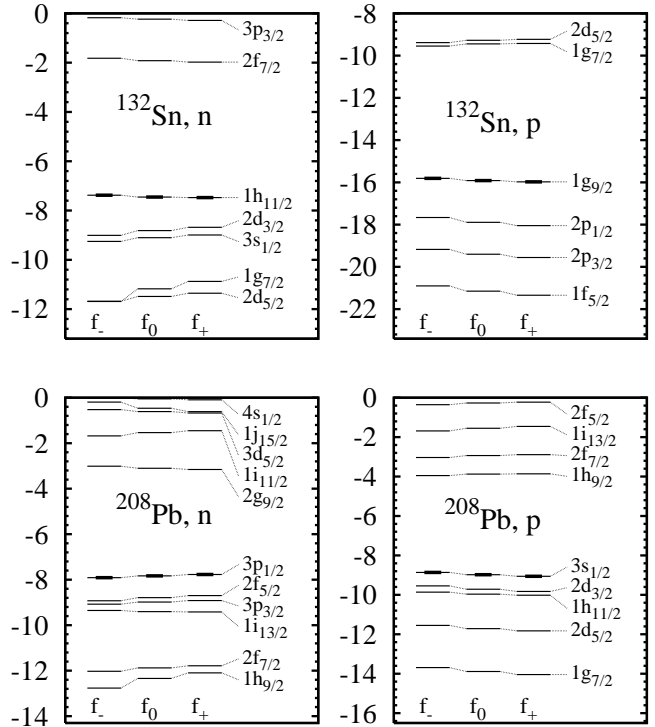


Figure 2: Single-particle energies [MeV] in ^{132}Sn and ^{208}Pb computed with indicated forces. Thick lines indicate the Fermi level ε_F .

Let us therefore examine similar spectra for more neutron-rich nuclei, *i.e.* ^{78}Ni ($I = 0.28$, experimentally observed [54]) and ^{156}Sn ($I = 0.36$). The ^{156}Sn nucleus is

used as an example of an extremely asymmetric system, even beyond the reach of planned radioactive beam facilities [55]. We observe on the lower right panel of Fig. 3 that the effect of Δm^* on proton single-particle energies at $Z = 50$ is more pronounced in ^{156}Sn than it was in ^{132}Sn . The modification of level densities appears quite clearly in ^{78}Ni also, while neutron levels around ε_F in ^{156}Sn are shifted in a slightly more disordered way.

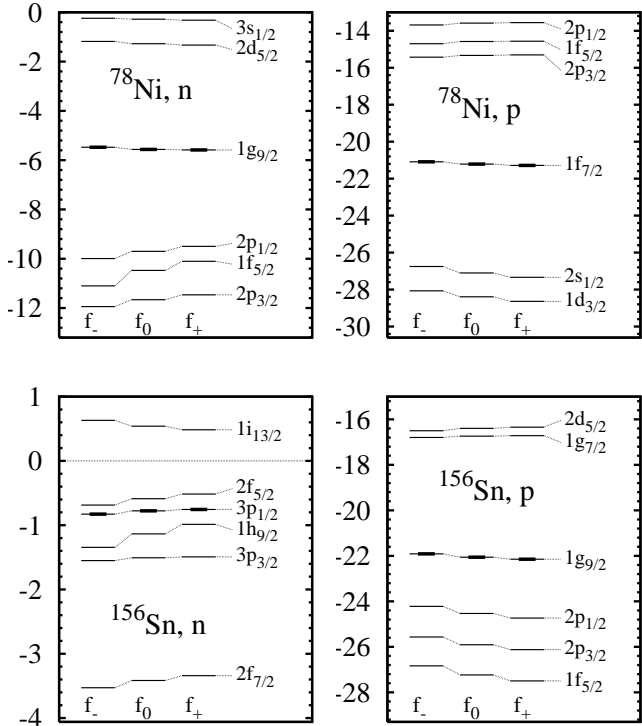


Figure 3: Same as Fig. 2 in ^{78}Ni and ^{156}Sn .

High- ℓ /low- n orbitals (n, ℓ being respectively the principal and orbital quantum numbers) are in fact more sensitive to variations of the spin-orbit field than to Δm^* because of their spatial localization near the surface of the nucleus. The spin-orbit field is modified between functionals by the interplay between J^2 -term coefficients and effective mass parameters, since these both depend on the same non-local terms of the Skyrme force [56]. The spin-orbit force ($\rho \nabla \cdot \mathbf{J}$ terms in the EDF), which is subject to a slight readjustment, does affect the spectra as well. We observed, overall, a marginal increase of the spin-orbit field strength when going from f_- to f_+ . This implies that while the global effect of modifying the level density is quite clearly observed when we alter the effective mass parameters, details of the spectroscopy are at least as sensitive to the terms connected to the spin-orbit field.

2. Pairing gaps

As an example, neutron spectral gaps are plotted on Fig. 4 for Sn and Pb series, up to the drip line, against experimental gaps extracted through five-point mass formulas [41, 53]. The slight change in the level density translates into a modification of the pairing gaps: a higher neutron effective mass (f_+) corresponds to a denser spectrum and higher gaps. The effect, which increases with asymmetry, remains however very small, because of the limited alteration of single-particle levels seen on Figs. 2 and 3.

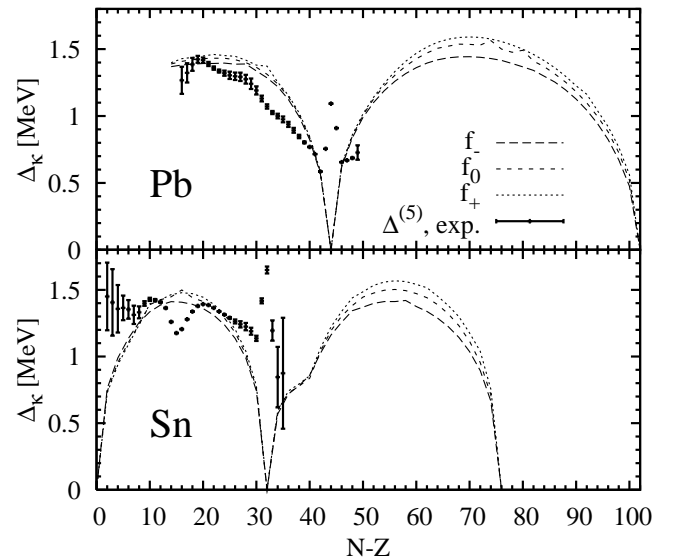


Figure 4: Neutron spectral gaps computed in Sn (bottom) and Pb (top) series with f_- , f_0 , f_+ , as a function of asymmetry. Experimental $\Delta^{(5)}$ gaps extracted from masses [57] are plotted with error bars.

In the end, the effect is negligible and would be overwhelmed by any other modification of the particle-hole part of the functional. For example the spin-orbit force, acting on the detailed level scheme, could alter the shape of gaps. The pairing functional itself is a subject of current debate regarding its density dependence, regularization scheme and finite-range corrections [58], while the HFB formalism can itself be improved (particle number projection) as well as the mere choice of observable to be compared (definition of theoretical and experimental gaps), although our choice has been proven to be possibly the most sound for extracting pure pairing effects [53].

3. Binding energies

Let us now study the effect of the aforementioned variation of level densities and pairing gaps on binding energies. On Fig. 5 we show the binding energy residuals $E_{\text{th}} - E_{\text{exp}}$ for Sn and Pb isotopes and $N = 50$ and

$N = 82$ isotones. The evolution of $E_{\text{th}} - E_{\text{exp}}$ along such series is usually plagued by an underbinding of open-shell nuclei with respect to closed-shell ones which translates into an arch shape of E -residual curves. Although the variation of m_v^* seems to impact the arches, again, the effect is negligible compared to the absolute value of deviations from experiment, except in the $N = 82$ series where open-shell nuclei tend to be more underbound in the case of f_+ .

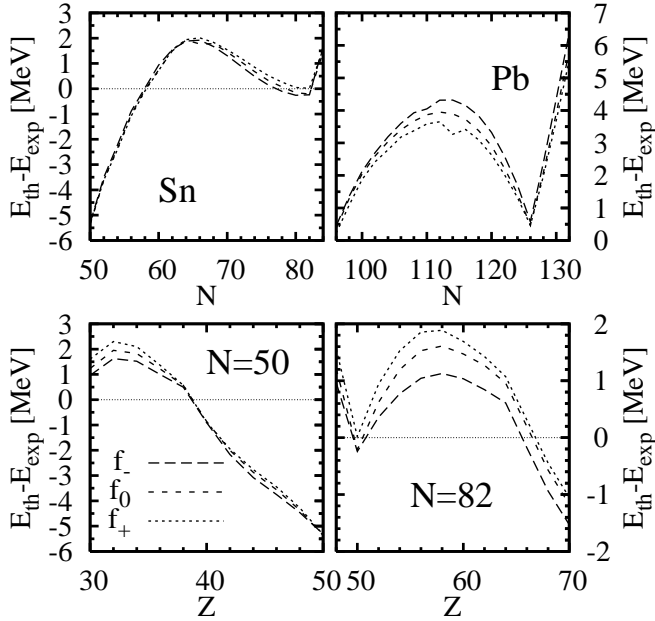


Figure 5: Binding energy residuals computed with forces f_- , f_0 and f_+ for semi-magic series of nuclei, as indicated.

4. Isovector giant resonances

The isovector effective mass is usually defined from the energy-weighted sum rule \mathfrak{m}_1 (the TRK sum rule [46]) of the isovector giant dipole resonance (IVGDR):

$$\mathfrak{m}_1(E1; T = 1) = \frac{\hbar^2}{2m} \frac{NZ}{A} (1 + \kappa_v) = \frac{\hbar^2}{2m} \frac{NZ}{A} \frac{m}{m_v^*}, \quad (7)$$

which exhibits its link with the strength distribution of isovector collective modes. We perform here a schematic study of dynamical properties of f_- , f_0 , f_+ by means of results derived in Ref. [59]. Thanks to RPA sum rules similar to Eq. (7), it is possible to fit an accurate parameterization of the energy $E_1 = \mathfrak{m}_1/\mathfrak{m}_{-1}$ of isovector giant resonances in a given nucleus as a function of Skyrme parameters. Results for GDR ($L = 1$) and isovector giant monopole (IVGMR, $L = 0$) modes in ^{208}Pb are shown in Table II, compared to experimental energies (respectively from Refs. [60] and [61] and corrected, as suggested in [59], for the shift due to the spreading of the strength by damping effects – 2 MeV for GMR, 1 MeV for GDR).

Table II: E_1 energies of ^{208}Pb isovector giant resonances computed thanks to a sum-rule parameterization (see text), compared to experimental energy centroids. Experimental uncertainties are as indicated. We infer from figures in Ref. [59] the accuracy of theoretical energies computed with the fits in that reference, with respect to full RPA calculations, to be of the order of 1 MeV.

κ_v	$E_1(L = 0, T = 1)$	$E_1(L = 1, T = 1)$
f_-	0.15	24.55
f_0	0.43	26.43
f_+	0.60	27.25
exp. centroid	26.3 ± 1.1	14.3 ± 0.1

While f_- predicts both energies lower than experimental ones, values for f_0 and f_+ are compatible with experiment for the $L = 0$ mode, and only f_+ approaches the experimental value for the $L = 1$ mode. This suggests that values of κ_v corresponding to a positive value of Δm^* (equal to or higher than 0.43 in our case) better describe isovector dynamics than lower values.

As a summary, the effect of the splitting of neutron and proton effective masses with isospin asymmetry on single-particle energies, pairing gaps and binding energies, is noticeable and consistent, yet limited and thus hardly meaningful when compared to the overall (in)accuracy of the predictions made by current nuclear EDF. In fact, the main reason for not seeing a dramatic modification of EDF predictions when altering Δm^* is the limited amount of strongly asymmetric nuclear matter at high enough density in the ground state of nuclei with realistic isospin as already suggested in [30]. This makes the effect of the isovector effective mass rather marginal. Giant isovector resonances are certainly more fruitful to seek for an effect of a modification of Δm^* . Indeed, a sum-rule-based analysis of isovector collective modes allows a slightly more clear-cut conclusion, with a tendency to favor $\Delta m^* \gtrsim 0$. The conclusion of the phenomenological study done in this section is that, while no observable listed here strongly ask for $\Delta m^* > 0$, there is no reason to omit this constraint in future functionals, since, as already stated, ab-initio predictions for the sign of Δm^* are solid. There remains to check the intrinsic consistency of the functional in terms of other ab-initio inputs and stability criteria.

III. FURTHER STUDY OF INFINITE MATTER

A. Separation of the EOS into (S, T) channels

1. Introduction

In this section, we discuss the contributions to the potential energy of SNM from the four two-body spin-isospin (S, T) channels. We compare our results with those predicted by BHF calculations [62] using AV18 [63]

two-body interaction and a three-body force constructed from meson exchange theory [64, 65].

Using projectors on spin singlet and triplet states, respectively

$$\hat{P}_{S=0} = \frac{1}{2}(1 - \hat{P}_\sigma), \quad \hat{P}_{S=1} = \frac{1}{2}(1 + \hat{P}_\sigma), \quad (8)$$

where \hat{P}_σ is the spin-exchange operator, and similar expressions for isospin projectors \hat{P}_T using the isospin exchange operator \hat{P}_τ , yields the potential energy in each (S, T) channel

$$E_{\text{pot}}^{ST} = \frac{1}{2} \sum_{kl} \left\langle kl \left| V \hat{P}_S \hat{P}_T \right| \bar{k}\bar{l} \right\rangle \rho_{kk} \rho_{ll}, \quad (9)$$

where the sum on k, l runs over all HF single-particle eigenstates whereas ρ_{kk} designates the diagonal one-body density matrix. The notation $|\bar{k}\bar{l}\rangle$ denotes a non-normalized but antisymmetrized two-body state. In order to compare different many-body approaches (ab-initio or EDF), we use the “potential energy” which refers to the total binding energy from which is subtracted the kinetic energy of the non-interacting particle system.

Note that due to the zero-range character of the Skyrme force, together with at most second-order derivative terms, only $L = 0, 1$ partial waves occur explicitly whereas higher partial waves contribute to ab-initio EOS. We find, for SNM,

$$\frac{E_{\text{pot}}^{00}}{A} = \frac{3}{160} t_2 (1 - x_2) \left(\frac{3\pi^2}{2} \right)^{2/3} \rho_0^{5/3}, \quad (10a)$$

$$\frac{E_{\text{pot}}^{10}}{A} = \frac{3}{16} \sum_{i=0}^2 t_{0i} (1 + x_{0i}) \rho_0^{1+i/3} + \frac{9}{160} t_1 (1 + x_1) \left(\frac{3\pi^2}{2} \right)^{2/3} \rho_0^{5/3}, \quad (10b)$$

$$\frac{E_{\text{pot}}^{01}}{A} = \frac{3}{16} \sum_{i=0}^2 t_{0i} (1 - x_{0i}) \rho_0^{1+i/3} + \frac{9}{160} t_1 (1 - x_1) \left(\frac{3\pi^2}{2} \right)^{2/3} \rho_0^{5/3}, \quad (10c)$$

$$\frac{E_{\text{pot}}^{11}}{A} = \frac{27}{160} t_2 (1 + x_2) \left(\frac{3\pi^2}{2} \right)^{2/3} \rho_0^{5/3}, \quad (10d)$$

where (t_i, x_i) are usual coefficients of the Skyrme EDF, whereas (t_{0i}, x_{0i}) characterize the density-independent zero-range term and the two density-dependent ones, following the parameterization of equation (A1).

The coefficients occurring in Eqs. (10a)–(10d) stem from the antisymmetrization condition $(-)^{L+S+T} = -1$, the relative angular momentum L being even for t_{0i} and $t_1(\mathbf{k}^2)$ terms and odd for $t_2(\mathbf{k}' \cdot \mathbf{k})$ terms. The expression of the potential energy in channels $(S, T) = (0, 0)$ and $(1, 1)$ is very simple since only the t_2 term contributes.

2. Force vs. functional

Previous statements, however, apply only to the case where the EDF is computed as the expectation value of an (antisymmetrized) effective force. In the more general case, it is still possible to define (S, T) channels starting from any Hartree-like functional. Indeed, the functional can always be expressed in terms of an effective non-antisymmetrized vertex and one can still plug a projector in the calculation of its matrix elements. In the pure functional case, there is however no more clear definition of partial waves, and spin-isospin channels emerge from the balance between coefficients of (iso)scalar/(iso)vector couplings (see appendix B for a more detailed discussion).

As long as there are not enough inputs to constrain *all* degrees of freedom of a general functional, the “force” approach remains as an acceptable path, and hence shall be used in the following.

3. Results

Results are plotted against BHF predictions on Fig. 6. First, one can observe that results are rather scattered. Second, the main source of binding, from $(S, T) = (0, 1)$ and $(1, 0)$ channels, is not well described and the detailed saturation mechanism is not captured. It is clear that, even though all four forces reproduce perfectly PNM and SNM EOS, they do not have the same spin-isospin content, and that the latter is in general rather poor. Thus, fitting the global EOS is an important element but it does not mean that spin-isospin properties of the functional are fixed once and for all. One needs to do more and fitting ab-initio predictions of $E_{\text{pot}}^{(S,T)}$ seems to be a good idea in the near future. However, one needs to make sure that the theoretical uncertainty of the data used is smaller than the expected accuracy of the fit to them. This calls for predictions from other ab-initio methods using the same two-body plus three-body Hamiltonian. Then, those ab-initio calculations should be repeated us-

ing different sets of two-body plus three-body Hamiltonians in order to provide a theoretical error bar on those predictions.

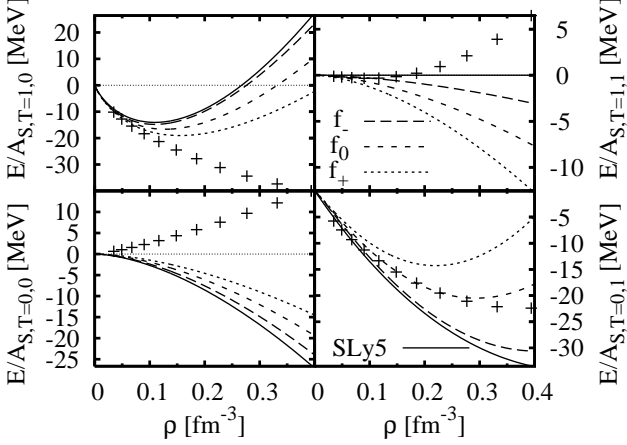


Figure 6: Energy per particle in each (S, T) channel for SNM, as a function of density. Crosses refer to the BHF calculations [62].

The most obvious discrepancy appears in $(0, 0)$ and $(1, 1)$ channels where Skyrme and BHF data have opposite signs above saturation density. The SLy5 parameter set shows a particular behavior in channel $(1, 1)$ due to the choice of $x_2 = -1$ to prevent ferromagnetic instabilities in PNM. Note that these two channels are taken care of, in the Skyrme functional, by the density-independent P -wave term only. The upper-right panel of Fig. 6 points out the tendency of Skyrme parameterizations to be attractive in polarized PNM, and hence to cause a collapse of its EOS at high density. At lower densities, BHF data show a distinctive behavior, being slightly attractive below ρ_{sat} and repulsive above. This feature cannot be matched by the standard Skyrme functional which exhibits a monotonous behavior as a function of density in this channel, regardless of the value of (t_2, x_2) .

It is also worth noticing that the failure in channel $(1, 1)$ becomes more and more prominent as one makes Δm^* closer to the ab-initio predictions (force f_+). The effective masses being governed by the momentum dependent terms of the force, it is not a surprise that the modification of the former impacts channels $(0, 0)$ and $(1, 1)$. What changes in the coefficients entering Eqs. (10a-10d) stems only from the variation of m_v^* and the associated rearrangement of parameters in the functional, most notably the $C_{0,1}^{\Delta\rho}$ coefficients closely related to surface and surface-symmetry energies. The relatively tight requirements on the latter imply that the four parameters of the non-local terms in the standard Skyrme energy functional would be dramatically overconstrained if we were to add the (S, T) -channel decomposition in the fitting data.

In the end, the rather poor properties of the functional in channels $(0, 0)$ and $(1, 1)$, the degradation of the latter as the effective mass splitting is improved, the idea of us-

ing ab-initio (S, T) contributions in the fit, call, at least, for a refinement of the odd- L term in the sense either of a density dependence or of a higher-order derivative term. The latter being prone to numerical instabilities and interpretation problems, a density-dependent $\mathbf{k}' \cdot \mathbf{k}$ term remains as one of the next potential enhancements to be brought to the Skyrme EDF (density-dependent derivative terms have been considered already, but with a focus on even- L terms of the form $t_4(\mathbf{k}^2 + \mathbf{k}'^2)\rho_0^\beta$ [66]). Phenomenological constraints on gradient terms are mainly related to the surface of nuclei, i.e. low-density regions. One can expect that, to first order, BHF data in channel $(S, T) = (1, 1)$ can be matched with an extended functional while retaining a good agreement with other (experimental) data. It is less clear in channel $(0, 0)$ but further exploration of the extended parameter space may bring Skyrme and BHF data in better agreement.

B. RPA linear response functions and the diagnosis of instabilities

We attempt here to study general stability conditions of SNM with respect to finite-size density, spin, isospin and spin-isospin perturbations. Our basic ingredient is the RPA response function [67] derived analytically in Ref. [68] for the central part of the Skyrme interaction. Recent work was done to incorporate the effect of the spin-orbit part which was found to be quite negligible [69], and will be omitted in the present work. One starts by defining a one-body perturbing operator

$$\mathcal{Q}^{(\alpha)} = e^{-i\omega t} \sum_a e^{i\mathbf{q} \cdot \mathbf{r}_a} \Theta_a^{(\alpha)}, \quad (11)$$

where a indexes particles in the system. The one-body spin-isospin operators $\Theta_a^{(\alpha)}$ are defined as

$$\Theta_a^{\text{ss}} = 1_a, \quad \Theta_a^{\text{vs}} = \boldsymbol{\sigma}_a, \quad \Theta_a^{\text{sv}} = \vec{\tau}_a, \quad \Theta_a^{\text{vv}} = \boldsymbol{\sigma}_a \vec{\tau}_a, \quad (12)$$

where we use the denomination of (iso-)scalar (s) and (iso-)vector (v) channels in order to distinguish the uncoupled spin-isospin channels from the coupled two-body (S, T) channels discussed in the previous section. In Eq. (12) and the following, the first (second) subscripts denotes the spin (isospin). We then study the response to each type of perturbation separately through the *response functions*

$$\begin{aligned} \chi^{(\alpha)}(\omega, \mathbf{q}) &= \frac{1}{\Omega} \sum_n |\langle n | \mathcal{Q}^{(\alpha)} | 0 \rangle|^2 \\ &\times \left(\frac{1}{\omega - E_{n0} + i\eta} - \frac{1}{\omega + E_{n0} - i\eta} \right), \end{aligned} \quad (13)$$

at the RPA level, where Ω stands for a normalization volume and $|n\rangle$ is an excited state of the system, E_{n0} being the corresponding energy. Since the central residual interaction does not couple the channels defined through

Eq. (12) in SNM, we can indeed consider each channel separately.

The response function $\chi^{(\alpha)}$ can be seen as the propagator of the collective perturbation, *i.e.* the positions of its poles in the (q, ω) plane yield the dispersion relation of the mode. In this formalism, the onset of an unstable mode is marked by the occurrence of a pole in $\chi^{(\alpha)}$ at $\omega = 0$, corresponding to zero excitation energy. Such a pole marks the transition between stable ($\chi^{(\alpha)} < 0$) and unstable ($\chi^{(\alpha)} > 0$) domains. Unstable modes of infinite wavelength ($q = 0$) are those traditionally discussed in the context of Landau parameters. A pole at finite q characterizes a system which is unstable with respect to the appearance of a spatial oscillation of a given type (density, spin, isospin or spin-isospin) with a given wavelength $\lambda = 2\pi/q$.

The evaluation of response functions calls for the residual interaction V_{p-h} , defined as the second-order functional derivative of the energy with respect to the density matrix. Its momentum-space matrix elements can be written, using total momentum conservation, as [68]:

$$V_{p-h}(\mathbf{q}_1, \mathbf{q}_2, \mathbf{q}) = \langle \mathbf{q}_1 \mathbf{q}_2 + \mathbf{q} | V_{p-h} | \mathbf{q}_1 + \mathbf{q} \mathbf{q}_2 \rangle, \quad (14)$$

$$= \hat{W}_1(q) + \hat{W}_2(q) (\mathbf{q}_1 - \mathbf{q}_2)^2, \quad (15)$$

with

$$\begin{aligned} \hat{W}_1(q) = \frac{1}{4} [& W_1^{ss}(q) + W_1^{vs}(q) \boldsymbol{\sigma}_1 \cdot \boldsymbol{\sigma}_2 + W_1^{sv}(q) \vec{\tau}_1 \circ \vec{\tau}_2 \\ & + W_1^{vv}(q) \boldsymbol{\sigma}_1 \cdot \boldsymbol{\sigma}_2 \vec{\tau}_1 \circ \vec{\tau}_2], \end{aligned} \quad (16)$$

and a similar expression for \hat{W}_2 . We find:

$$\frac{W_1^{ss}(q)}{4} = 2C_0^{\rho,0} + \sum_{i=1}^2 C_0^{\rho,i} \frac{(i+6)(i+3)}{9} \rho_0^{i/3} - 2C_0^{\Delta\rho} \mathbf{q}^2, \quad (17a)$$

$$\frac{W_1^{vs}(q)}{4} = 2C_0^{s,0} + 2 \sum_{i=1}^2 C_0^{s,i} \rho_0^{i/3} - 2C_0^{\Delta s} \mathbf{q}^2, \quad (17b)$$

$$\frac{W_1^{sv}(q)}{4} = 2C_1^{\rho,0} + 2 \sum_{i=1}^2 C_1^{\rho,i} \rho_0^{i/3} - 2C_1^{\Delta\rho} \mathbf{q}^2, \quad (17c)$$

$$\frac{W_1^{vv}(q)}{4} = 2C_1^{s,0} + 2 \sum_{i=1}^2 C_1^{s,i} \rho_0^{i/3} - 2C_1^{\Delta s} \mathbf{q}^2, \quad (17d)$$

$$\frac{W_2^{ss}(q)}{4} = C_0^\tau, \quad (18a)$$

$$\frac{W_2^{vs}(q)}{4} = C_0^{sT}, \quad (18b)$$

$$\frac{W_2^{sv}(q)}{4} = C_1^\tau, \quad (18c)$$

$$\frac{W_2^{vv}(q)}{4} = C_1^{sT}. \quad (18d)$$

With the above expression for the residual interaction, the response function reads as

$$\begin{aligned} \chi^{(\alpha)}(\omega, \mathbf{q}) = 4\Pi_0 \left[& 1 - W_1^{(\alpha)} \Pi_0 - 2W_2^{(\alpha)} k_F^2 \left(\bar{q}^2 - \frac{\nu^2}{1 - \frac{m^* k_F^3}{3\pi^2} W_2^{(\alpha)}} \right) \Pi_0 \right. \\ & \left. + 2W_2^{(\alpha)} k_F^2 (2\bar{q}^2 \Pi_0 - \Pi_2) + (W_2^{(\alpha)} k_F^2)^2 \left(\Pi_2^2 - \Pi_0 \Pi_4 + 4\bar{q}^2 \nu^2 \Pi_0^2 - \frac{2m^* k_F}{3\pi^2} \bar{q}^2 \Pi_0 \right) \right]^{-1}, \end{aligned} \quad (19)$$

where $\bar{q} = q/2k_F$, $\nu = \omega m_s^*/qk_F$ and $\Pi_{0,2,4}$ are generalized Lindhard functions, see Ref. [68].

As already said, the limit $\mathbf{q} \rightarrow 0$ corresponds to perturbations of infinite wavelength, keeping the system homogeneous. There, the residual interaction is uniquely determined by Landau parameters F_l, F'_l, G_l, G'_l , with $l = 0, 1$, and well known stability conditions are obtained under the form [70]:

$$1 + \frac{X_l}{2l+1} > 0, \quad (20)$$

where X_l represents any of the Landau parameters. We have used this criterion in the fit of our forces f_x , ensuring that no spin or spin-isospin instability would occur

below $2\rho_{\text{sat}}$. We observe that, from the point of view of Landau parameters, the most critical channel is the vector-isovector one, with associated instabilities at densities as low as $2\rho_{\text{sat}}$ (see the upper-right panel of Fig. 9). This behavior is linked to the attractive character of the functional in channel $(S, T) = (1, 1)$ which gives rise to a collapse of spin-polarized PNM, and accordingly, a vanishing spin-isospin symmetry energy. Therefore, better reproducing the decomposition into (S, T) channels of EOS obtained from ab-initio methods is not only a matter of microscopic motivation, but also a necessity to avoid unwanted instabilities.

Beyond infinite wavelength instabilities, we also aim at demonstrating that a more general treatment is needed

Table III: Values of the $C_1^{\Delta\rho}$ coefficient, in MeV fm⁵.

	f_-	SLy5	f_0	f_+	LNS	SkP
Δm^*	-0.284	-0.182	0.001	0.170	0.227	0.418
$C_1^{\Delta\rho}$	5.4	16.7	21.4	29.4	33.75	35.0

to fully describe and control unstable modes which arise in the Skyrme EDF framework. Thus, contributions to the residual interaction coming from functional terms of the form $\rho\Delta\rho$ are zero for $\mathbf{q} = 0$, whereas such terms drive finite-size instabilities.

Indeed, we have observed that existing (SkP) or new parameterizations built with a high value of κ_v in order to reproduce the microscopic splitting of effective masses, tend to spatially separate protons from neutrons in spherical mean-field calculations, where enough iterations lead to states with strongly oscillating densities and a diverging energy. Following a preliminary phenomenological reasoning, we could relate this effect to the $C_1^{\Delta\rho}\vec{\rho}_1 \cdot \Delta\vec{\rho}_1$ term in the functional, as this term can energetically favor strong oscillations of the isovector density $\vec{\rho}_1$ which arise in the case of such a spatial n-p separation. Moreover, Eqs. (17a-18d) show that such a term can yield an attractive contribution to the residual interaction in the case of a short-wavelength (high q) perturbation. We found empirically that parameter sets for which this instability arises are characterized by a high value of $C_1^{\Delta\rho}$, that is $C_1^{\Delta\rho} \gtrsim 30$. As seen from Table III, this parameter is strongly correlated with the effective mass splitting Δm^* in such a way that a positive splitting, as required by ab-initio predictions, leads to instabilities.

Whereas we were obviously unable to provide a fully converged (and hence physically meaningful) and clearly unstable force to illustrate the previous statements, we found that certain forces available in the literature present the aforementioned behavior. For example, convergence problems have arisen (and have already been pointed out in another study [71]) for the SkP parameter set [45]. The nature of the instabilities discussed here is illustrated on the lower panels of Fig. 7, where neutron and proton densities are plotted at various stages of execution of a self-consistent iterative procedure with SkP in ^{56}Ni . We see that strong, opposing oscillations of neutron and proton densities are formed, and steadily increase with iterations. Such a behavior happens after a seemingly converged situation for which the relative energy variation is small but almost constant over a large number of iterations and the evolution of the energy is monotonous.

The study of the linear response function in the scalar-isovector channel allows us to provide a more quantitative ground to the previous observation. By plotting critical densities (lowest density of occurrence of a pole in

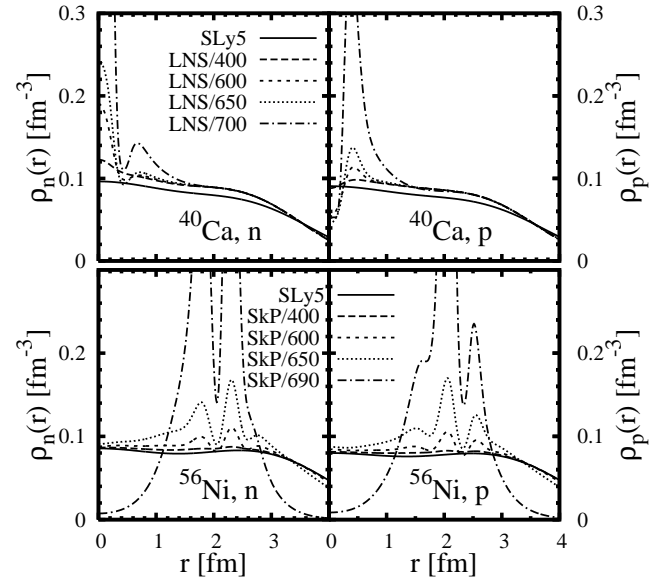


Figure 7: Neutron and proton densities in central regions of ^{56}Ni (bottom) and ^{40}Ca (top) plotted for a fully converged computation using the SLy5 force (solid line; relative variation of energy between iterations less than 10^{-14}) and along a series of iterations done with SkP (bottom) and LNS (top). Number of iterations as indicated in key. In both cases the collapse happens after a seemingly converged situation ($\sim 10^{-9}$ relative energy variation, steady over a large number of iterations indicating a nearly linear evolution of the energy), which can be mistaken for an energy minimum if too loose a convergence criterion is used.

$\chi^{(\alpha)}(\omega = 0, q)$) for a given q on Fig. 8, we see that these critical densities can be very close to ρ_{sat} for $q \approx 2.5$ to 3 fm^{-1} . This is the case for SkP, which displays the lowest scalar-isovector critical density of all forces studied in this paper. Accordingly, it is the most prone to a lack of convergence in HF calculations.

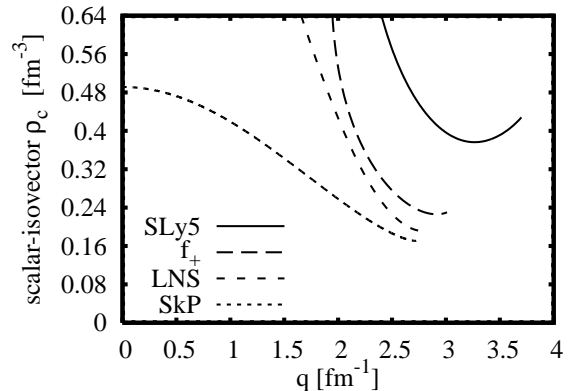


Figure 8: The lowest density of occurrence of a pole in $\chi^{sv}(\omega = 0, \mathbf{q})$ is plotted against the wave-number q of the scalar-isovector perturbation. The curves end at $q = 2k_F$ since the ground state can not couple to excitations with $\omega = 0, q > 2k_F$.

The link between response functions and convergence problems can indeed be understood by classifying them by their magnitude: in case of a stable but very soft mode, lack of convergence arises from the existence of a continuum of quasi-degenerate mean-field states, among which no minimization or self-consistency algorithm shall be able to decisively find an energy minimum without a considerable amount of iterations. If the soft mode becomes unstable, it causes a divergence of the energy and of other observable such as the densities. We see in the agreement between the RPA study of SNM and the observation of unstable HF calculations of nuclei a qualitative validation of our Local Density Approximation (LDA)-based treatment of instabilities: soft or unstable modes occurring in INM happen for the same parameter sets in finite nuclei.

The large number of iterations needed for the divergence to occur on Fig. 7 is a consequence of the limiting case embodied by SkP, such that the existence of a definite instability is highly dependent on finite size effects (choice of the nucleus) and discretization details in the numerical procedure. If SkP is a limiting case, LNS also displays a low critical density in the scalar-isovector channel (Fig. 8). In this case, we observed proton-neutron separation in ^{40}Ca and for small mesh steps (0.1 fm) only (see Fig. 7), while it is more frequent with SkP. Our force f_+ , with a critical density just slightly higher than LNS, successfully passed the test of computing a series of 134 spherical nuclei. This again demonstrates that testing finite-size instabilities through response functions constitutes an accurate tool, the critical density (and its proximity to ρ_{sat}) being a good measure of the gravity of the problems one might encounter in finite nuclei. Although the actual occurrence of instabilities is subject to details of the numerical treatment, it is now clear that their origin can be traced back to the choice of parameters in the functional itself.

Nevertheless, even if a functional does not display clear instabilities but only spurious soft collective modes, convergence difficulties shall arise in mean-field calculations while such a mode will translate into a non-physical low-lying spectrum in a beyond-mean-field framework. This can then yield excessive correlation energies if one systematically includes correlations in the ground state *e.g.* in (Q)RPA or GCM methods. One should thus make sure that no spurious (even remotely) soft mode occurs at saturation density in order to prevent such problems.

Having demonstrated the importance of finite-size instabilities, let us go back to discussing our original set of forces and perform a generalization to other spin-isospin channels.

Critical densities are plotted on Fig. 9 for the four channels defined in Eq. (12). The upper-left panel shows that, while no unstable mode occurs at $q = 0$ thanks to fitting PNM EOS to relatively high density, scalar-isovector instabilities may happen little above ρ_{sat} for $q \approx 2.5$ to 3 fm^{-1} . In addition, there is a clear trend for lowering the critical density when Δm^* is increased,

in agreement with the preliminary phenomenological reasoning on $C_1^{\Delta\rho}$.

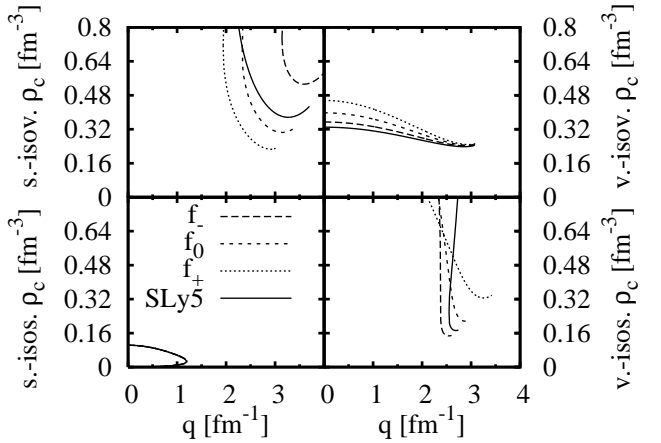


Figure 9: Same as Fig. 8, for all spin-isospin channels. The lower-left panel shows the region of spinodal instabilities below ρ_{sat} . The domain of q covered in this case determines the size of structures formed, while the region between 0.1 and 0.16 fm^{-1} appears as metastable.

Spin channels have been taken care of during the fit thanks to Landau parameters, which describe the residual interaction at $q = 0$. The result can be seen on the right panels of Fig. 9, where the critical densities of instability are plotted for spin-flip modes (isoscalar and isovector). As previously stated, the most dangerous $q = 0$ instability is found in the vector-isovector channel. By looking at the upper-right panel of Fig. 9 one can see that the critical density is even lower ($1.5\rho_{\text{sat}}$) at $q = 3 \text{ fm}^{-1}$ than at $q = 0$, a domain not covered by the criterion of Eq. (20).

An even more prominent finite-size effect can be observed in the isoscalar spin-flip channel (lower-right panel of Fig. 9) where, while no instability occurs at $q = 0$ as in the case of most Skyrme forces, finite-size instabilities occur at low density, even below ρ_{sat} ! These instabilities are linked to the $C_0^{\Delta s} \mathbf{s}_0 \cdot \Delta \mathbf{s}_0$ term which makes the vector-isoscalar V_{p-h} attractive at large q whereas it is repulsive at $q = 0$. Values of $C_0^{\Delta s}$, indeed, are as high as 45.85 and 47.32 for SLy5 and f_- , respectively. As a consequence, one can expect divergences in calculations of odd or rotating nuclei with the latter forces if the aforementioned terms are included. In this case, though, increasing Δm^* pushes the critical density farther from ρ_{sat} : f_0 and f_+ functionals are thus the only ones to be free from instabilities at ρ_{sat} , without being totally satisfactory either.

The previous discussion is valid if the full time-odd functional is taken into account. This must be stressed since $\mathbf{s}_0 \cdot \Delta \mathbf{s}_0$ terms, which drive the most critical, finite-size instabilities, have never been included in self-consistent mean field calculations to date. However, RPA calculations are commonly performed by computing

the residual interaction matrices directly from the antisymmetrized force (plus rearrangement terms), which amounts to implicitly including the contribution to V_{p-h} from all terms in the functional [72].

The latter findings finalize the picture of a competition between spin and isospin instabilities. All in all, the strong interplay between the various quantities linked to the four parameters of the non-local terms in the Skyrme force does not seem to allow for a fully satisfactory compromise between stability criteria and ab-initio constraints on Δm^* . Again, we see that the non-local part of the Skyrme force is too simplistic to control all relevant properties. An extension with density- and momentum-dependent terms, allowing the fine-tuning of the functional at various densities, combined with the formal checks advocated in this paper, could prove to significantly improve the predictive power of Skyrme EDF.

IV. CONCLUSION

We have built a series of Skyrme energy density functionals to study the effect of a variation of the splitting of neutron and proton effective masses with isospin asymmetry on properties of this mean-field-based model. Thanks to the use of a second density-dependent term in the underlying effective force, we could cover a wide range of effective mass splittings (Δm^*) with a satisfactory fit to nuclear properties. Indeed, nuclear observable predicted by our functionals f_- , f_0 and f_+ show a remarkable similarity, pointing out that spectra, pairing gaps and masses of bound nuclei are weakly sensitive to Δm^* , mostly due to their relatively low isospin asymmetry. Although observable were affected in a noticeable and consistent way, no clear improvement was seen when altering Δm^* either way.

Beyond this phenomenological study, we have compared the splitting of the equation of state of symmetric infinite matter into spin-isospin channels provided by our functionals and by ab-initio Brueckner-Hartree-Fock calculations. Such a comparison showed an obvious discrepancy in $(S, T) = (0, 0)$ and $(1, 1)$ channels, where energies predicted by Skyrme functionals and by BHF calculations have opposite signs. The inconsistency in channel $(S, T) = (1, 1)$, where the Skyrme functional is attractive, translates into a collapse of polarized neutron matter EOS, related to the onset of spin-isospin instabilities at quite low density ($2\rho_{\text{sat}}$). In this channel, ab-initio predictions cannot be matched (in the Skyrme “force” approach) without an extension of the P-wave term. We also identified finite-size isospin instabilities caused by strong isovector gradient terms, which prevent the convergence of mean-field calculations. We were able to provide a firm and quantitative basis to these observations through an analysis of finite-size instabilities by use of RPA linear response functions in SNM. The latter showed that finite-size effects in the analysis of instabilities tend to always dominate.

The present study leads us to propose the systematic inclusion of consistency checks with ab-initio predictions of spin-isospin properties in the construction of our future functionals, as well as a systematic diagnosis of finite-size instabilities.

Acknowledgments

Work by K. B. was performed within the framework of the Espace de Structure Nucléaire Théorique (ESNT). The authors are grateful to D. Lacroix for a careful reading of the manuscript and helpful comments and also thank M. Bender and B. Cochot for valuable discussions during the development of this study. Two of us (K. B. and T. L.) wish to thank the NSCL for its hospitality during final stages of this work. This work was supported by the U.S. National Science Foundation under Grant No. PHY-0456903.

Appendix A: SKYRME ENERGY FUNCTIONAL

We take the particle-hole part of the functional as given by the expectation value of a Skyrme effective force including two density-dependent terms:

$$\begin{aligned} V(\mathbf{R}, \mathbf{r}) = & \sum_{i=0}^2 t_{0i} \left(1 + x_{0i} \hat{P}_\sigma \right) \delta(\mathbf{r}) [\rho_0(\mathbf{R})]^{i/3} \\ & + \frac{1}{2} t_1 \left(1 + x_1 \hat{P}_\sigma \right) [\delta(\mathbf{r}) \mathbf{k}^2 + \mathbf{k}'^2 \delta(\mathbf{r})] \\ & + t_2 \left(1 + x_2 \hat{P}_\sigma \right) \mathbf{k}' \cdot \delta(\mathbf{r}) \mathbf{k} \\ & + iW_0 [\boldsymbol{\sigma}_1 + \boldsymbol{\sigma}_2] \mathbf{k}' \times \delta(\mathbf{r}) \mathbf{k}, \end{aligned} \quad (\text{A1})$$

with the usual notations

$$\mathbf{R} = (\mathbf{r}_1 + \mathbf{r}_2) / 2, \quad (\text{A2a})$$

$$\mathbf{r} = \mathbf{r}_1 - \mathbf{r}_2, \quad (\text{A2b})$$

$$\mathbf{k} = \frac{1}{2i} (\nabla_1 - \nabla_2), \quad (\text{A2c})$$

$$\mathbf{k}' = \text{C.C. of } \mathbf{k} \text{ acting on the left}, \quad (\text{A2d})$$

$$\boldsymbol{\sigma} = \boldsymbol{\sigma}_1 + \boldsymbol{\sigma}_2, \quad (\text{A2e})$$

$$\hat{P}_\sigma = \frac{1}{2} (1 + \boldsymbol{\sigma}_1 \cdot \boldsymbol{\sigma}_2). \quad (\text{A2f})$$

The total binding energy of a nuclear system can be written as a functional of a local energy density

$$E = \int d^3\mathbf{r} \mathcal{H}(\mathbf{r}), \quad (\text{A3})$$

$$\mathcal{H} = \frac{\hbar^2}{2m} \tau_0 + \mathcal{H}_{\text{Skyrme}} + \mathcal{H}_{\text{Coul.}}, \quad (\text{A4})$$

$$\mathcal{H}_{\text{Skyrme}} = \mathcal{H}_0^{\text{even}} + \mathcal{H}_1^{\text{even}} + \mathcal{H}_0^{\text{odd}} + \mathcal{H}_1^{\text{odd}}, \quad (\text{A5})$$

where the superscripts in the last equation indicate the behavior with respect to time reversal of densities occurring in each term, while subscripts indicate the rank of

the densities in isospin space. The corresponding expressions are

$$\mathcal{H}_0^{\text{even}} = C_0^\rho \rho_0^2 + C_0^{\Delta\rho} \rho_0 \Delta \rho_0 + C_0^\tau \rho_0 \tau_0 + C_0^J \mathbb{J}_0^2 + C_0^{\nabla J} \rho_0 \nabla \cdot \mathbf{J}_0, \quad (\text{A6a})$$

$$\mathcal{H}_1^{\text{even}} = C_1^\rho \vec{\rho}_1^2 + C_1^{\Delta\rho} \vec{\rho}_1 \cdot \Delta \vec{\rho}_1 + C_1^\tau \vec{\rho}_1 \cdot \vec{\tau}_1 + C_1^J \vec{\mathbb{J}}_1^2 + C_1^{\nabla J} \vec{\rho}_1 \cdot \nabla \cdot \vec{\mathbf{J}}_1, \quad (\text{A6b})$$

$$\mathcal{H}_0^{\text{odd}} = C_0^s \mathbf{s}_0^2 + C_0^{\Delta s} \mathbf{s}_0 \cdot \Delta \mathbf{s}_0 + C_0^{sT} \mathbf{s}_0 \cdot \mathbf{T}_0 + C_0^{\nabla s} (\nabla \cdot \mathbf{s}_0)^2 + C_0^j \mathbf{j}_0^2 + C_0^{\nabla j} \mathbf{s}_0 \cdot (\nabla \times \mathbf{j}_0), \quad (\text{A6c})$$

$$\mathcal{H}_1^{\text{odd}} = C_1^s \vec{\mathbf{s}}_1^2 + C_1^{\Delta s} \vec{\mathbf{s}}_1 \cdot \Delta \vec{\mathbf{s}}_1 + C_1^{sT} \vec{\mathbf{s}}_1 \cdot \vec{\mathbf{T}}_1 + C_1^{\nabla s} (\nabla \cdot \vec{\mathbf{s}}_1)^2 + C_1^j \vec{\mathbf{j}}_1^2 + C_1^{\nabla j} \vec{\mathbf{s}}_1 \cdot (\nabla \times \vec{\mathbf{j}}_1). \quad (\text{A6d})$$

Bold letters denote vector densities and arrows denote isovector densities. Neutron and proton densities ($q = +1$ for neutrons, $q = -1$ for protons) are thus given by

$$\begin{aligned} \rho_q(\mathbf{r}) &= \frac{1}{2} (\rho_0 + q \rho_{1,3}), \\ \tau_q(\mathbf{r}) &= \frac{1}{2} (\tau_0 + q \tau_{1,3}), \\ \mathbb{J}_q(\mathbf{r}) &= \frac{1}{2} (\mathbb{J}_0 + q \mathbb{J}_{1,3}), \end{aligned} \quad (\text{A7})$$

with similar expressions for time-odd densities. The spin-current vector \mathbf{J}_t is built from the antisymmetric part of tensor \mathbb{J}_t .

Let us give the expressions, in terms of Skyrme force parameters, of the coupling constants entering the HFB calculations which are altered by the addition of a second density-dependent term

$$C_0^\rho = \sum_{i=0}^2 C_0^{\rho,i} \rho_0^{i/3} = \sum_{i=0}^2 \frac{3}{8} t_{0i} \rho_0^{i/3}, \quad (\text{A8a})$$

$$\begin{aligned} C_1^\rho &= \sum_{i=0}^2 C_1^{\rho,i} \rho_0^{i/3} \\ &= \sum_{i=0}^2 -\frac{1}{8} t_{0i} (1 + 2x_{0i}) \rho_0^{i/3}, \end{aligned} \quad (\text{A8b})$$

as well as the constants related, respectively, to isoscalar and isovector effective masses,

$$C_0^\tau = \frac{1}{16} [3t_1 + t_2(5 + 4x_2)], \quad (\text{A9a})$$

$$C_1^\tau = \frac{1}{16} [-t_1(1 - 2x_1) + t_2(1 + 2x_2)], \quad (\text{A9b})$$

and constants multiplying gradient terms discussed in sec. III B,

$$C_0^{\Delta\rho} = \frac{1}{64} [-9t_1 + t_2(5 + 4x_2)], \quad (\text{A10a})$$

$$C_1^{\Delta\rho} = \frac{1}{64} [3t_1(1 + 2x_1) + t_2(1 + 2x_2)], \quad (\text{A10b})$$

$$C_0^{\Delta s} = \frac{1}{64} [3t_1(1 - 2x_1) + t_2(1 + 2x_2)], \quad (\text{A10c})$$

$$C_1^{\Delta s} = \frac{1}{64} [3t_1 + t_2]. \quad (\text{A10d})$$

The expressions of all other coupling constants are given in Ref. [1]. Some of the above constants are linked through the gauge invariance of the functional, related to the Galilean invariance of the underlying effective force:

$$C_t^j = -C_t^\tau, \quad C_t^J = -C_t^{sT}, \quad C_t^{\nabla j} = C_t^{\nabla J}. \quad (\text{A11})$$

The densities used above can be written as functionals of the density matrix expressed in coordinate space, *i.e.*

$$\hat{\rho}(\mathbf{x}\sigma q, \mathbf{x}'\sigma' q') = \sum_k \langle k | \mathbf{x}'\sigma' q' \rangle \langle \mathbf{x}\sigma q | k \rangle \rho_{kk}, \quad (\text{A12})$$

as

$$\begin{aligned} \rho_0(\mathbf{r}) &= \int d^3\mathbf{x} d^3\mathbf{x}' \sum_{\sigma\sigma'qq'} \delta(\mathbf{r} - \mathbf{x}) \delta(\mathbf{x}' - \mathbf{x}) \delta_{q'q} \delta_{\sigma'\sigma} \\ &\times \hat{\rho}(\mathbf{x}\sigma q, \mathbf{x}'\sigma' q'), \end{aligned} \quad (\text{A13a})$$

$$\begin{aligned} \Delta\rho_0(\mathbf{r}) &= \int d^3\mathbf{x} d^3\mathbf{x}' \sum_{\sigma\sigma'qq'} \delta(\mathbf{r} - \mathbf{x}) \delta(\mathbf{x}' - \mathbf{x}) \delta_{q'q} \delta_{\sigma'\sigma} \\ &\times (\nabla'^2 + 2\nabla' \cdot \nabla + \nabla^2) \hat{\rho}(\mathbf{x}\sigma q, \mathbf{x}'\sigma' q'), \end{aligned} \quad (\text{A13b})$$

$$\begin{aligned} \tau_0(\mathbf{r}) &= \int d^3\mathbf{x} d^3\mathbf{x}' \sum_{\sigma\sigma'qq'} \delta(\mathbf{r} - \mathbf{x}) \delta(\mathbf{x}' - \mathbf{x}) \delta_{q'q} \delta_{\sigma'\sigma} \\ &\times \nabla' \cdot \nabla \hat{\rho}(\mathbf{x}\sigma q, \mathbf{x}'\sigma' q'), \end{aligned} \quad (\text{A13c})$$

$$\begin{aligned} \mathbb{J}_0(\mathbf{r}) &= \int d^3\mathbf{x} d^3\mathbf{x}' \sum_{\sigma\sigma'qq'} \delta(\mathbf{r} - \mathbf{x}) \delta(\mathbf{x}' - \mathbf{x}) \delta_{q'q} \\ &\times \frac{1}{2i} (\nabla - \nabla') \otimes \sigma_{\sigma'\sigma} \hat{\rho}(\mathbf{x}\sigma q, \mathbf{x}'\sigma' q'), \end{aligned} \quad (\text{A13d})$$

$$\begin{aligned} \mathbf{j}_0(\mathbf{r}) &= \int d^3\mathbf{x} d^3\mathbf{x}' \sum_{\sigma\sigma'qq'} \delta(\mathbf{r} - \mathbf{x}) \delta(\mathbf{x}' - \mathbf{x}) \delta_{q'q} \delta_{\sigma'\sigma} \\ &\times \frac{1}{2i} (\nabla - \nabla') \hat{\rho}(\mathbf{x}\sigma q, \mathbf{x}'\sigma' q'), \end{aligned} \quad (\text{A13e})$$

where σ, σ' are indices referring to spin, q and q' refer to isospin, ∇ is the gradient operator acting on the coordinate x , ∇' being the same acting on x' . Isovector and other time-odd densities can be expressed by replacing, respectively, $\delta_{q'q}$ by $\vec{\tau}_{q'q}$ and $\delta_{\sigma'\sigma}$ by $\sigma_{\sigma'\sigma}$ where appropriate.

Appendix B: SEPARATION OF THE ENERGY INTO SPIN-ISOSPIN CHANNELS

When the EDF is defined as the expectation value of an effective Hamiltonian, separating it into spin-isospin channels is straightforward, as in Eq. (9). However, one can extend this definition to the case of any Hartree-like functional: let us start by recalling that in the case of the Skyrme force, the direct and exchange terms have the same analytical structure; one thus usually uses the expressions

$$E_{\text{pot}} = \frac{1}{2} \sum_{kl} \langle kl | V_{\text{Skyrme}} | \overline{kl} \rangle \rho_{kk} \rho_{ll}, \quad (\text{B1})$$

$$| \overline{kl} \rangle = | kl \rangle - | lk \rangle = (1 - \hat{P}_r \hat{P}_\sigma \hat{P}_\tau) | kl \rangle, \quad (\text{B2})$$

where the last expression uses the position, spin and isospin exchange operators to define an antisymmetrized and non-normalized two-body state. One then writes down the antisymmetrized form of Eq. (A1) and the EDF

by using the definition of densities entering Eqs. (A6a)-(A6d).

Leaving the antisymmetrized Hamiltonian framework, it is always possible to define the potential part of the functional as the *direct term* of the expectation value of a certain operator, as in

$$E_{\text{pot}} = \sum_{kl} \langle kl | V_{\text{EDF}} | kl \rangle \rho_{kk} \rho_{ll}, \quad (\text{B3})$$

recalling that $V_{\text{EDF}} = V_{\text{Skyrme}}(1 - \hat{P}_r \hat{P}_\sigma \hat{P}_\tau)$ in the Hamiltonian case. One then defines the energy per channel as

$$E_{\text{EDF}}^{ST} = \sum_{kl} \left\langle kl \left| V_{\text{EDF}} \hat{P}_S \hat{P}_T \right| kl \right\rangle \rho_{kk} \rho_{ll}, \quad (\text{B4})$$

which, with the definitions (A6a)-(A6d) for coupling constants, yields (retaining only terms acting in infinite matter)

$$E_{\text{pot}}^{ST} = \int d^3r \mathcal{H}^{ST}(\mathbf{r}) \quad (\text{B5})$$

$$\begin{aligned} \mathcal{H}^{ST} = & [C_0^\rho + (4S-3)C_0^s + (4T-3)C_1^\rho + (4S-3)(4T-3)C_1^s] \\ & \times \frac{1}{16} [(2S+1)(2T+1)\rho_0^2 + (2S-1)(2T+1)\mathbf{s}_0^2 + (2S+1)(2T-1)\vec{\rho}_1^2 + (2S-1)(2T-1)\vec{\mathbf{s}}_1^2] \\ & + [C_0^\tau + (4S-3)C_0^{sT} + (4T-3)C_1^\tau + (4S-3)(4T-3)C_1^{sT}] \\ & \times \frac{1}{16} [(2S+1)(2T+1)\rho_0\tau_0 + (2S-1)(2T+1)\mathbf{s}_0 \cdot \mathbf{T}_0 + (2S+1)(2T-1)\vec{\rho}_1\vec{\tau}_1 + (2S-1)(2T-1)\vec{\mathbf{s}}_1 \cdot \vec{\mathbf{T}}_1]. \end{aligned} \quad (\text{B6})$$

Appendix C: PARTICLE-HOLE RESIDUAL INTERACTION

With the definition of densities given in Eqs. (A13b)-(A13e) the particle-hole residual interaction is obtained through

$$\begin{aligned} & \langle \mathbf{x}'_1 \sigma'_1 q'_1, \mathbf{x}'_2 \sigma'_2 q'_2 | V_{\text{p-h}} | \mathbf{x}_1 \sigma_1 q_1, \mathbf{x}_2 \sigma_2 q_2 \rangle \\ & = \frac{\delta^2 \mathcal{E}}{\delta \rho(\mathbf{x}_1 \sigma_1 q_1, \mathbf{x}'_1 \sigma'_1 q'_1) \delta \rho(\mathbf{x}_2 \sigma_2 q_2, \mathbf{x}'_2 \sigma'_2 q'_2)}, \end{aligned} \quad (\text{C1})$$

which, for the central, spin-scalar, isoscalar part of the functional, *i. e.*

$$\mathcal{H}^{\text{sv}} = C_0^\rho(\rho_0) \rho_0^2 + C_0^{\Delta\rho} \rho_0 \Delta \rho_0 + C_0^\tau (\rho_0 \tau_0 - \mathbf{j}_0^2), \quad (\text{C2})$$

(the generalization to the full central part, omitted here for the sake of brevity, being straightforward), reads

$$\begin{aligned} V_{\text{p-h}} = & 2C_0^{\rho,0} + \sum_{i=1}^2 C_0^{\rho,i} \left(\frac{i}{3} + 2 \right) \left(\frac{i}{3} + 1 \right) \rho_0^{i/3} \\ & + C_0^\tau \left(\nabla'_1 \cdot \nabla_1 + \nabla'_2 \cdot \nabla_2 \right. \\ & \left. + \frac{1}{2} (\nabla'_1 - \nabla_1) \cdot (\nabla'_2 - \nabla_2) \right) \\ & + C_0^{\Delta\rho} \left((\nabla'_1)^2 + 2\nabla'_1 \cdot \nabla_1 + \nabla_1^2 \right. \\ & \left. + (\nabla'_2)^2 + 2\nabla'_2 \cdot \nabla_2 + \nabla_2^2 \right). \end{aligned} \quad (\text{C3})$$

When computing the momentum-space matrix element, Eq. (14), one makes the substitutions $\nabla_1 = i(\mathbf{q}_1 + \mathbf{q})$, $\nabla_2 = i\mathbf{q}_2$, $\nabla'_1 = -i\mathbf{q}_1$ and $\nabla'_2 = -i(\mathbf{q}_2 + \mathbf{q})$ (with $\hbar = 1$), which yields expressions (17a)-(18d).

[1] M. Bender, P.-H. Heenen, and P.-G. Reinhard, Rev. Mod. Phys. **75**, 121 (2003).

[2] E. Chabanat, P. Bonche, P. Haensel, J. Meyer, and R. Schaeffer, Nucl. Phys. **A627**, 710 (1997).

[3] E. Chabanat, P. Bonche, P. Haensel, J. Meyer, and R. Schaeffer, Nucl. Phys. **A635**, 231 (1998).

[4] E. Chabanat, P. Bonche, P. Haensel, J. Meyer, and R. Schaeffer, Nucl. Phys. **A643**, 441 (1998).

[5] J. M. Lattimer and M. Prakash, Science **304**, 536 (2004).

[6] L.-W. Chen, C. M. Ko, and B.-A. Li, Phys. Rev. Lett. **94**, 032701 (2005).

[7] S. Typel and B. A. Brown, Phys. Rev. C **64**, 027302 (2001).

[8] B.-A. Li, Phys. Rev. C **69**, 064602 (2004).

[9] B.-A. Li, C. B. Das, S. D. Gupta, and C. Gale, Phys. Rev. C **69**, 011603 (2004).

[10] H. Bethe, Rev. Mod. Phys. **62**, 801 (1990).

[11] M. Farine, J. M. Pearson, and F. Tondeur, Nucl. Phys. **A696**, 396 (2001).

[12] I. Bombaci and U. Lombardo, Phys. Rev. C **44**, 1892 (1991).

[13] S. Kubis and M. Kutschera, Phys. Lett. **B399**, 191 (1997).

[14] W. Zuo, I. Bombaci, and U. Lombardo, Phys. Rev. C **60**, 024605 (1999).

[15] V. Greco, M. Colonna, M. D. Toro, G. Fabbri, and F. Matera, Phys. Rev. C **64**, 045203 (2001).

[16] F. Hofmann, C. Keil, and H. Lenske, Phys. Rev. C **64**, 034314 (2001).

[17] B. Liu, V. Greco, V. Baran, M. Colonna, and M. D. Toro, Phys. Rev. C **65**, 045201 (2002).

[18] J. Rizzo, M. Colonna, M. D. Toro, and V. Greco, Nucl. Phys. **A732**, 202 (2004).

[19] Z.-Y. Ma, J. Rong, B.-Q. Chen, Z.-Y. Zhu, and H.-Q. Song, Phys. Lett. **B604**, 170 (2004).

[20] E. van Dalen, C. Fuchs, and A. Faessler, Phys. Rev. Lett. **95**, 022302 (2005).

[21] W. Satula, R. A. Wyss, and M. Rafalski, Phys. Rev. C **74**, 011301 (2006).

[22] M. Bender, J. Dobaczewski, J. Engel, and W. Nazarewicz, Phys. Rev. C **65**, 054322 (2002).

[23] J. P. Jeukenne, A. Lejeune, and C. Mahaux, Phys. Rep. **25**, 83 (1976).

[24] M. Baldo, *Nuclear methods and the nuclear equation of state*, Int. Rev. Nucl. Phys., Vol 9 (World Scientific, Singapore, 1999).

[25] W. Kohn and L. J. Sham, Phys. Rev. **137**, A1697 (1964).

[26] J. P. Blaizot and D. Gogny, Nucl. Phys. **A284**, 429 (1977).

[27] A. P. Severyukhin, C. Stoyanov, V. V. Voronov, and Nguyen Van Giai, Phys. Rev. C **66**, 034304 (2002).

[28] J. Meyer, P. Bonche, M. S. Weiss, J. Dobaczewski, H. Flocard, and P.-H. Heenen, Nucl. Phys. **A588**, 597 (1995).

[29] V. Bernard and Nguyen Van Giai, Nucl. Phys. **A348**, 75 (1980).

[30] S. Goriely, M. Samyn, M. Bender, and J. M. Pearson, Phys. Rev. C **68**, 054325 (2003).

[31] K. F. Liu and Nguyen Van Giai, Phys. Lett. **B65**, 23 (1976).

[32] R. J. Charity, L. G. Sobotka, and W. H. Dickhoff (2006), nucl-ex/0605026.

[33] A. M. Lane, Nucl. Phys. **35**, 676 (1962).

[34] F. Sammarruca, W. Barredo, and P. Krastev, Phys. Rev. C **71**, 064306 (2005).

[35] C. M. M. Jaminon, Phys. Rev. C **40**, 354 (1989).

[36] M. Bender, K. Rutz, P.-G. Reinhard, J. A. Maruhn, and W. Greiner, Phys. Rev. C **60**, 034304 (1999).

[37] A. T. Kruppa, M. Bender, W. Nazarewicz, P.-G. Reinhard, T. Vertse, and S. Cwiok, Phys. Rev. C **61**, 034313 (2000).

[38] M. Bender, W. Nazarewicz, and P.-G. Reinhard, Phys. Lett. **B515**, 42 (2001).

[39] J.-F. Berger, L. Bitaud, J. Dechargé, M. Girod, and K. Dietrich, Nucl. Phys. **A685 (1-4)**, 1c (2001).

[40] N. Paar, T. Nikšić, D. Vretenar, and P. Ring, Phys. Lett. **B606**, 288 (2005).

[41] T. Duguet, P. Bonche, P.-H. Heenen, and J. Meyer, Phys. Rev. C **65**, 014310 (2002).

[42] C. Rigollet, P. Bonche, H. Flocard, and P.-H. Heenen, Phys. Rev. C **59**, 3120 (1999).

[43] B. Cochet, K. Bennaceur, P. Bonche, T. Duguet, and J. Meyer, Nucl. Phys. **A731**, 34 (2004).

[44] L. G. Cao, U. Lombardo, C. W. Shen, and Nguyen Van Giai, Phys. Rev. C **73**, 014313 (2006).

[45] J. Dobaczewski, H. Flocard, and J. Treiner, Nucl. Phys. **A422**, 103 (1984).

[46] O. Bohigas, A. M. Lane, and J. Martorell, Phys. Rep. **51**, 267 (1979).

[47] G. F. Bertsch, B. Sabbey, and M. Uusnaki, Phys. Rev. C **71**, 054311 (2005).

[48] M. Beiner, H. Flocard, Nguyen Van Giai, and P. Quentin, Nucl. Phys. **A238**, 29 (1975).

[49] J. Bartel, P. Quentin, M. Brack, C. Guet, and H.-B. Håkansson, Nucl. Phys. **A386**, 79 (1982).

[50] F. Chappert, M. Girod, and J.-F. Berger (2006), private communication.

[51] A. Akmal, V. R. Pandharipande, and D. G. Ravenhall, Phys. Rev. C **58**, 1804 (1998).

[52] A. Bulgac and Y. Yu, Phys. Rev. Lett. **88**, 042504 (2002).

[53] T. Duguet, P. Bonche, P.-H. Heenen, and J. Meyer, Phys. Rev. C **65**, 014311 (2002).

[54] P. T. Hosmer, H. Schatz, A. Aprahamian, O. Arndt, R. R. C. Clement, A. Estrade, K.-L. Kratz, S. N. Liddick, P. F. Mantica, W. F. Mueller, et al., Phys. Rev. Lett. **94**, 112501 (2005).

[55] *Physics case of spiral 2* (2006), <http://www.ganil.fr/>.

[56] J. Dobaczewski (2006), nucl-th/0604043.

[57] G. Audi, A. H. Wapstra, and C. Thibault, Nucl. Phys. **A739**, 337 (2003).

[58] T. Duguet and K. Bennaceur (2006), in preparation.

[59] G. Colò, Nguyen Van Giai, and H. Sagawa, Phys. Lett. **B363**, 5 (1995).

[60] J. Ritman, F.-D. Berg, W. Kühn, V. Metag, R. Novotny, M. Notheisen, P. Paul, M. Pfeiffer, O. Schwalb, H. Löhner, et al., Phys. Rev. Lett. **70**, 533 (1993).

[61] A. Erell, J. Alster, J. Lichtenstadt, M. A. Moinester, J. D. Bowman, M. D. Cooper, F. Irom, H. S. Matis, E. Piasetzky, and U. Sennhauser, Phys. Rev. C **34**, 1822 (1986).

[62] M. Baldo (2006), private communication.

[63] R. B. Wiringa, V. G. J. Stocks, and R. Schiavilla, Phys. Rev. C **51**, 38 (1995).

- [64] P. Grangé, A. Lejeune, M. Martzolff, and J.-F. Mathiot, Phys. Rev. C **40**, 1040 (1989).
- [65] A. Lejeune, U. Lombardo, and W. Zuo, Phys. Lett. **B477**, 45 (2000).
- [66] M. Farine and J. M. P. F. Tondeur, Nucl. Phys. **A615**, 135 (1997).
- [67] A. Fetter and J. D. Walecka, *Quantum Theory of Many-Particle Systems* (McGraw-Hill, New-York, 1971).
- [68] C. García-Recio, J. Navarro, Nguyen Van Giai, and N. N. Salcedo, Ann. of Phys. **214**, 293 (1992).
- [69] J. Margueron, J. Navarro, and Nguyen Van Giai (2006), unpublished, nucl-th/0604019.
- [70] A. B. Midgal, *Theory of Finite Fermi Systems and Applications to Atomic Nuclei* (Wiley, New York, 1967).
- [71] J. Terasaki and J. Engel (2006), nucl-th/0608007.
- [72] J. Terasaki, J. Engel, M. Bender, J. Dobaczewski, W. Nazarewicz, and M. Stoitsov, Phys. Rev. C **71** (2005).